International Journal of Minerals, Metallurgy and Materials
Volume 28, Number 4, April 2021, Page 729
https://doi.org/10.1007/s12613-020-2138-5

Growth mechanism and photocatalytic evaluation of flower-like ZnO microstructures prepared with SDBS assistance

Hong-mei Shao[1)], *Xiao-yi Shen*[2)], *Xue-tian Li*[1)], *Yong Cui*[1)], *Wei Zhang*[1)], *Wen-di Xu*[1)], *Zhong-cai Shao*[1)], *and Yu-chun Zhai*[2)]

1) School of Environmental and Chemical Engineering, Shenyang Ligong University, Shenyang 110159, China
2) School of Metallurgy, Northeastern University, Shenyang 110819, China
(Received: 3 May 2020; revised: 15 June 2020; accepted: 7 July 2020)

Abstract: Flower-like ZnO microstructures were successfully produced using a hydrothermal method employing $ZnSO_4$/$(NH_4)_2SO_4$ as a raw material. The effect of the operating parameters of the hydrothermal temperature, OH^-/Zn^{2+} molar ratio, time, and amount of dispersant on the phase structure and micromorphology of the ZnO particles were investigated. The synthesis conditions of the flower-like ZnO microstructures were: hydrothermal temperature of 160°C, OH^-/Zn^{2+} molar ratio of 5:1, reaction time of 4 h, and 4 mL of dispersant. The flower-like ZnO microstructures were comprised of hexagon-shaped ZnO rods arranged in a radiatively. Degradation experiments of Rhodamine B with the flower-like ZnO microstructures demonstrated a degradation efficiency of 97.6% after 4 h of exposure to sunshine, indicating excellent photocatalytic capacity. The growth mechanism of the flower-like ZnO microstructures was presented.

Keywords: flower-like ZnO microstructures; hydrothermal process; photocatalytic capacity; growth mechanism

1. Introduction

Microscale and nanoscale materials are of great interest because of their optical, catalyzing, and thermotic characteristics that are different from their bulk form [1–2]. ZnO is a promising material and widely applied in the fields of ceramics, pigments, rubbers, photocatalysis, and semiconductors [3–4]. To date, many methods have been employed to synthesize ultrafine ZnO, among which the hydrothermal method is an effective and simple technology for synthesizing ZnO with good crystallinity, controllable morphology, and narrow size distribution [5–8]. In a hydrothermal environment, ultrafine ZnO is self-assembles to produce a homogenous structure [9–10]. In addition, hydrothermal synthesis is a valuable method for the preparation of CuO and $ZnFe_2O_4$ nanostructures because of the control within the method and ability to produce a well-defined size [11–12]. Furthermore, the formation of three dimensional ZnO structures with excellent performance and a large specific surface area is the key to improvement [7].

In the most recent decade, dye waste pollution characterized by its high toxicity, and difficult degradation even at low concentration has become a serious problem worldwide because of rapid urbanization and development of the textile industry [13–14]. Various efforts, such as flocculation, membrane separation, absorption, and biodegradation, have been attempted to resolve and alleviate this pollution [15–16]. However, none completely eliminated the pollutants without additional limitations [16–17]. For example, membrane separation has high efficiency, but the operating cost is high [16–18]. Absorption is a low-cost and effective method, but the difficulty in recycling and the absorption capacity of the absorbents limit its application [16–18]. Photocatalysis is a promising solution because it can effectively oxidize a large amount of organic contaminants into relatively harmless inorganics [17,19–20]. Various metal and multi-metal oxides, such as TiO_2, Fe_2O_3, CuO, SnO_2, ZnO, WO_3, $BiVO_4$, and Bi_2WO_2, have been used in photocatalytic degradation [21–27]. Among them, ZnO is a crucial semiconductor with a band gap width of 3.37 eV and a high exciton binding energy of 60 meV [28]. Additionally, ZnO as a photocatalyst has advantages of high photosensitivity, controllable morphology, low-cost, and environmental friendliness [29–30]. Thus, ZnO receives considerable attention and it is universally accepted that ZnO particles with a three-dimensional structure exhibit better photocatalytic activity [31–32]. Polymeric and ceram-

Corresponding author: Hong-mei Shao E-mail: shaohm@sylu.edu.cn

ic membranes filled with ZnO nanostructures and pure ZnO membranes prepared using ZnO nanowires and nanotubes have been created and used in water treatments to eliminate organic pollutants, even heavy metal ions [7]. Additionally, ZnO nanostructures have potential in the fields of optoelectronic devices and dye-sensitized solar cells [8].

Although there are many efforts to enhance the photocatalytic properties of ZnO, including morphology control, nonmetallic and metallic elements/oxides doping/ coupling, and surface modification. However, there are two inevitable problems, the corrosion resistance of the ZnO photocatalyst and difficult recovery. Furthermore, the commonly used raw materials are $Zn(Ac)_2$ and $Zn(NO_3)_2$ with polyethylene glycol (PEG) as the dispersant. $ZnSO_4$ and zinc oxidized ore are rarely used. In order to address these drawbacks and realize the comprehensive utilization of zinc oxidized ore, a systematic investigation was conducted including zinc extraction, ZnO particle preparation, preparation of a corrosion-resistant film coating, and formation of magnetic core-shell composites. The objective of this work was to synthesize flower-like ZnO microstructures, evaluate the photocatalytic degradation capability by degrading Rhodamine B (RhB) in sunshine, and to provide reference data for the evaluation of the photocatalytic performance and potential of the composites.

2. Experimental

2.1. Materials

The $ZnSO_4/(NH_4)_2SO_4$ solution used as a raw material was obtained from zinc oxidized ore after multiple processing sequences of mixing with $(NH_4)_2SO_4$, roasting, water leaching, and removal of Fe and Al. The main components in the zinc oxidized ore (from Lanping) are ZnO (smithsonite and willemite), SiO_2 (quartz and Zn_2SiO_4), Fe_2O_3 (hematite), PbO (cerusite and anglesite), and CaO (limestone and gypsum) in contents of 25.36wt%, 21.05wt%, 18.12wt%, 4.70wt%, and 3.39wt%, respectively. The solution was adjusted to a specified Zn^{2+} concentration of 1 mol·L^{-1}. Analytic grade sodium hydroxide and sodium dodecyl benzene sulfonate (SDBS) were used as the precipitant and dispersant, respectively. The distilled water was homemade.

2.2. Procedure

An equal volume of 70 mL of 1 mol·L^{-1} $ZnSO_4/(NH_4)_2SO_4$ and pre-made 3, 5, and 7 mol·L^{-1} NaOH solutions were poured into a 200 mL Teflon reactor, respectively. Next, 2, 4, 6, or 8 mL of the SDBS solution with a mass fraction of 5% were added under magnetic stirring. The closed autoclave filled with a homogeneous mixed solution was placed in a pre-heated oven ranging from 140 to 180°C holding for a certain time (2 to 6 h). After the reaction, the autoclave was cooled and the slurry was filtered. The product was washed with distilled water repeatedly and twice with ethyl alcohol, dried at 100°C for 10 h to produce the ZnO powder.

Photocatalytic degradation experiments were performed under similar conditions on a sunny day from 10:00 to 15:00 on a windowsill. The intensity of the sunshine illumination was approximately (175–180) $\times 10^3$ lx. To determine the amount of ZnO, a 50 mL beaker was used as the reaction vessel. Flower-like ZnO (100 to 400 mg) was mixed with 20 mL of 10 to 25 mg·L^{-1} RhB solution, magnetically stirred for 20 min under darkness prior to testing, and then exposed to sunshine within 4.5 h. For the exposure time study, 50 mL solutions with appropriate ZnO powder were consumed in each test. Samples of 3–5 mL were collected and centrifuged at preset time intervals of 0.5 h. The absorbency of the diluted filtrates was measured three times and the average value was obtained.

3. Results and discussion

3.1. Influence of the hydrothermal temperature

The influence of the hydrothermal temperature on the phase structure and micromorphology of the ZnO powder under conditions of a OH^-/Zn^{2+} ratio of 5:1, a time of 4 h, and 4 mL of SDBS solution was studied, as shown in Fig. 1. The X-ray diffraction (XRD) results in Fig. 1(a) show that the position and intensity of the diffraction peaks were consistent with a hexagonal wurtzite structure (JCPDS files No. 361451) with good crystallinity. The influence of the temperature on the ZnO phase structure was negligible, but the effect on the morphology was significant. Flower-like ZnO observed by scanning electron microscopy (SEM) was recorded in Figs. 1(b) and 1(c), but that ZnO in Fig. 1(c) was more regular with an average particle size of 3 μm that was comprised of ZnO rods 2 μm in length oriented radiatively. The ZnO particles obtained at 180°C were hexagonal prisms and no flower-like structure was observed. The increased temperature promotes more regular flower-like ZnO structures. However, the excessive temperature enhances the excessive growth of ZnO rods, resulting in the destruction of the flower-like structures. To this end, a temperature of 160°C was used for further study.

3.2. Influence of the OH^-/Zn^{2+} ratio

The effect of the OH^-/Zn^{2+} molar ratio on the phase structure and micromorphology of the ZnO particles was studied under conditions of 160°C, a time of 4 h, and 4 mL of SDBS solution. As shown in Fig. 2, flower-like ZnO with a hexagonal wurtzite structure was prepared. Flower-like ZnO structures prepared at a OH^-/Zn^{2+} ratio of 3 (Fig. 2(b)) were composed of inhomogeneous flake and rod-like particles. The flower-like structures prepared at a OH^-/Zn^{2+} molar ratio of 5:1 (Fig. 2(c)) were more regular and uniform than that at a ratio of 3 (Fig. 2(b)). The ZnO rods grew radiatively to pro-

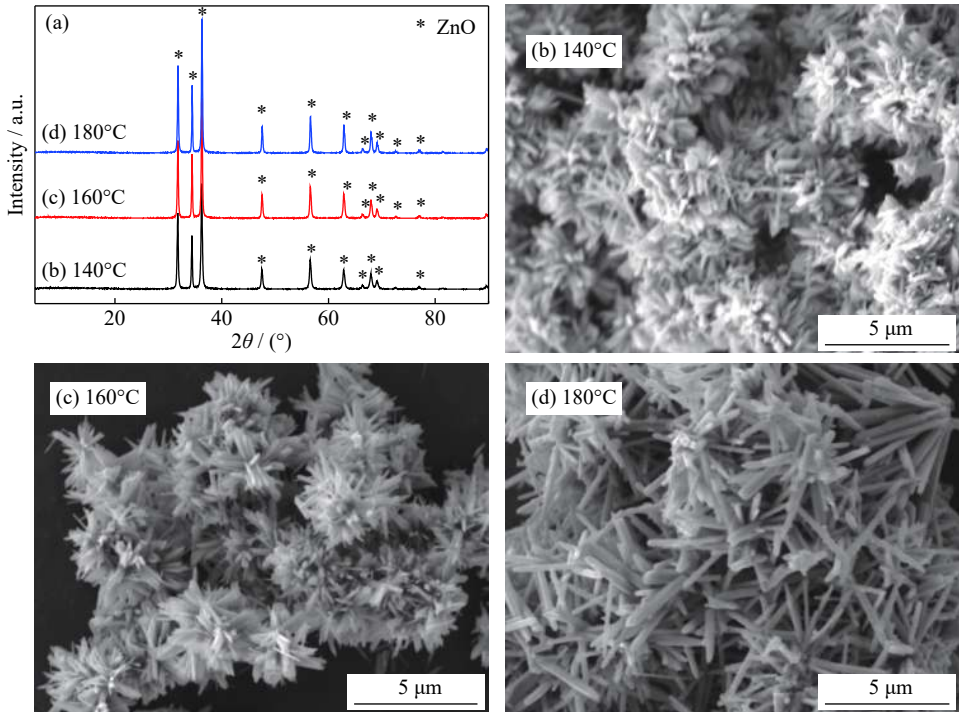

Fig. 1. XRD patterns (a) and SEM images of ZnO powders prepared at (b) 140°C, (c) 160°C, and (d) 180°C.

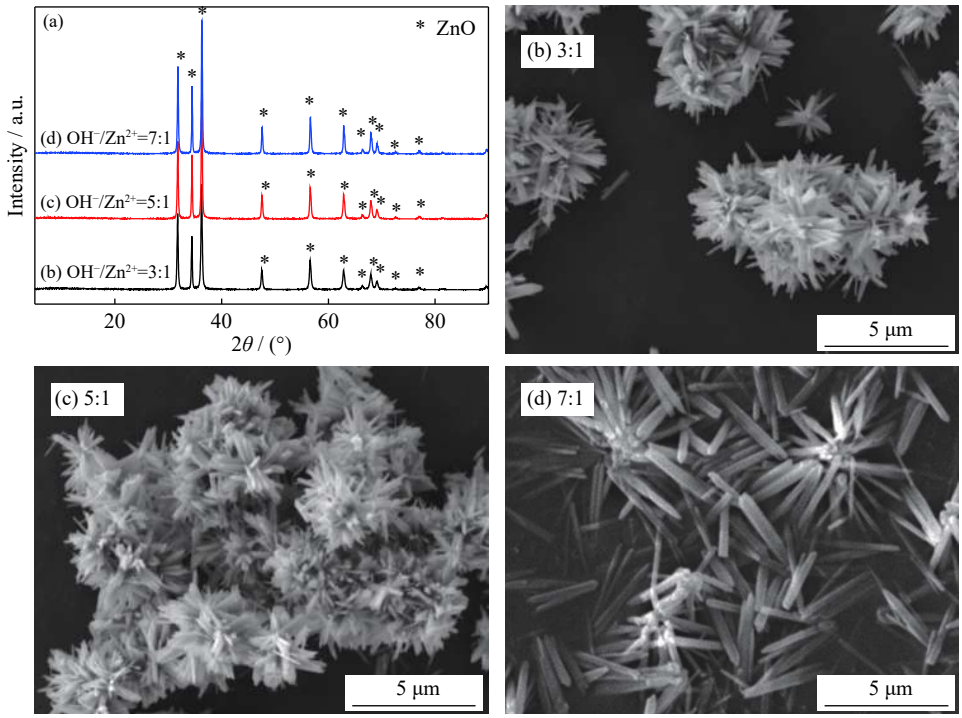

Fig. 2. XRD patterns (a) and SEM images of ZnO powders prepared at OH^-/Zn^{2+} ratio of (b) 3, (c) 5, and (d) 7.

duce a flower-like structure. The ZnO rods grew larger with increasing OH^-/Zn^{2+} ratio. At a OH^-/Zn^{2+} ratio of 7:1, the ZnO rods grew too large such that the flower-like morphology was destructed, leaving residual (Fig. 2(d)). The OH^-/Zn^{2+} molar ratio had a significant effect on the ZnO morphology. The strong polarity of the NaOH solution increases with an increase in the OH^-/Zn^{2+} molar ratio and the self-organizing growth ability of the ZnO particles was enhanced [1]. As a result, a OH^-/Zn^{2+} molar ratio of 5:1 was chosen.

3.3. Influence of the hydrothermal time

The experiments to evaluate the influence of the hydrothermal time on the phase structure and micromorphology of ZnO were performed at 160°C, a OH^-/Zn^{2+} ratio of 5:1, and 4 mL of SDBS solution, as shown in Fig. 3. All of the ZnO particles had a hexagonal wurtzite structure. Flower-like ZnO microstructures were observed in Figs. 3(b) and 3(c). Though the ZnO particles in Fig. 3(b) were flower-like and composed of short rod-like particles, the ZnO was still growing. The flower-like ZnO in Fig. 3(c) was regular. A long hydrothermal time produced adequate growth of ZnO rods. The micro-rods growing for 6 h were too long, overgrowing the flower-like structures and producing crossed rods (Fig. 2(d)). As a result, a time of 4 h was chosen.

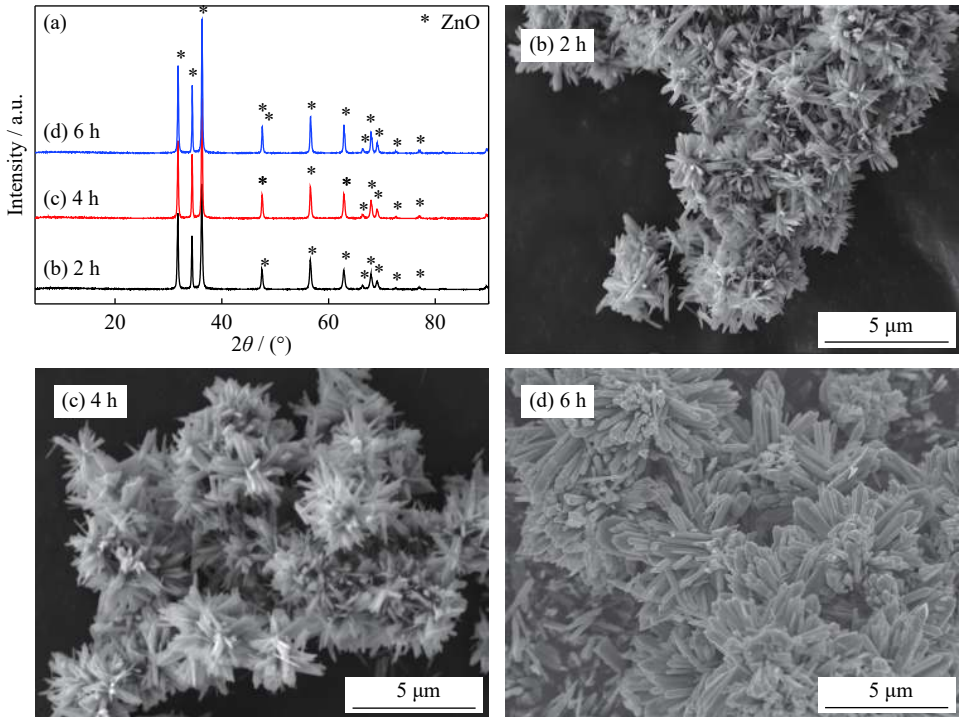

Fig. 3. XRD patterns (a) and SEM images of ZnO powders prepared at (b) 2 h, (c) 4 h, and (d) 6 h.

3.4. Influence of the amount of dispersant

The effect of the amount of dispersant on the phase structure and micromorphology of the ZnO powder evaluated at 160°C, a OH^-/Zn^{2+} ratio of 5:1, and a time of 4 h is shown in Fig. 4. The ZnO powders are a hexagonal wurtzite structure. ZnO particles obtained with 2 mL of SDBS solution were agglomerated flake particles (Fig. 4(b)). The ZnO particles in Fig. 4(c) exhibited irregular cluster-like structures with uneven rod sizes. Regular flower-like ZnO microstructures were observed in Fig. 4(d), but the ZnO rod length varied from 1 to 5 μm. As an anionic surface active agent, SDBS ($C_{18}H_{29}SO_3Na$) can form bundles of micelles and release Na^+ in solution. Negatively-charged bundles of micelles are attracted to the positively-charged Zn^{2+} in solution, which may affect the dehydration of $Zn(OH)_4^{2-}$ and promote ZnO rod growth agglomeration, leading to uniform growth of ZnO crystals. Excessive dispersant promotes ZnO rod growth so that the uniform flower-like structures are destructed. As a result, 4 mL of the SDBS solution was chosen.

Overall, the parameters for preparing flower-like ZnO microstructures were a hydrothermal temperature of 160°C, a OH^-/Zn^{2+} molar ratio of 5:1, a time of 4 h, and 4 mL of a 5% mass fraction SDBS solution.

3.5. Photocatalytic capacity of ZnO

The photocatalytic capacity of flower-like ZnO was examined by altering the ZnO amount and adjusting the RhB concentration. Fig. 5(a) displays the relationship between the degradation efficiency of RhB and exposure time by degrading 20 mL of the 10 $mg \cdot L^{-1}$ RhB solution with different amounts of ZnO. The unchanged RhB in darkness without ZnO shows that the self-degradation of RhB is inappreciable. Prolonged exposure time promotes the degradation efficiency of RhB. The degradation efficiency of RhB increases within the first 300 mg of ZnO and then decreases with more ZnO. The degradation efficiency of RhB reached a maximum value of 97.2% when the ZnO additive amount was 300 mg.

Under sunlight, the oxidizing reaction mainly occurs on the interface between ZnO active sites and RhB molecules

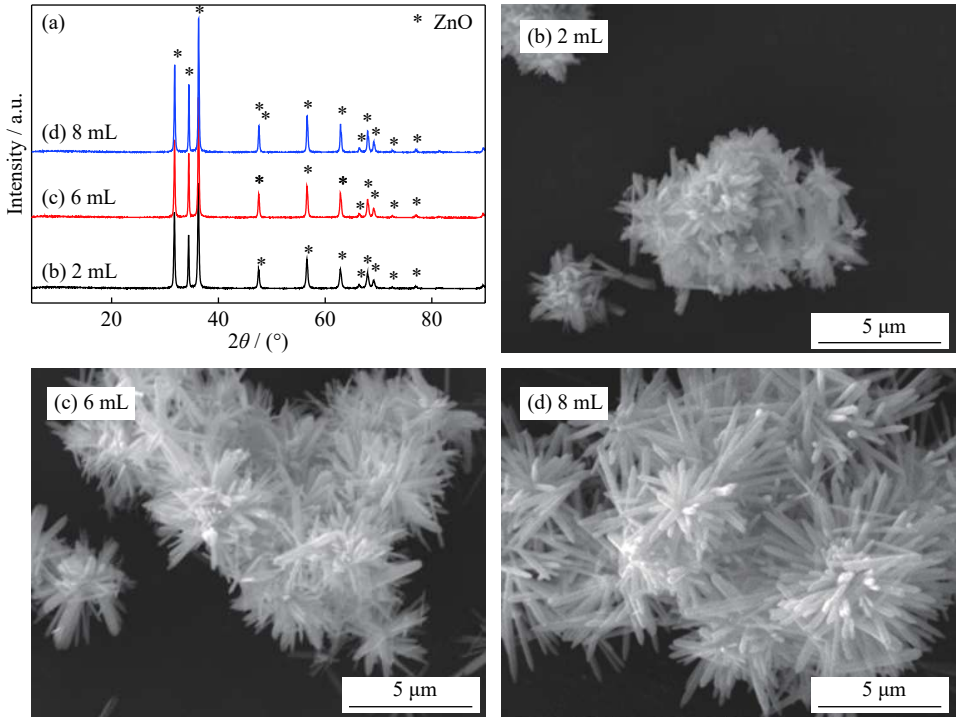

Fig. 4. XRD patterns (a) and SEM images of ZnO powders prepared at SDBS amount of (b) 2 mL, (c) 6 mL, and (d) 8 mL.

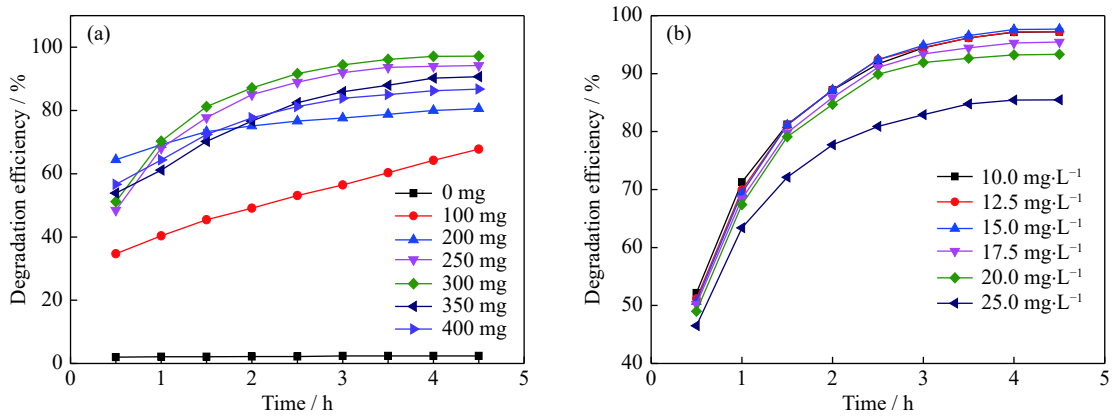

Fig. 5. Relationships between the degradation efficiency of RhB and time at different (a) ZnO amounts and (b) RhB concentrations.

because of the close contact [2,13]. Excessive addition of ZnO reduces the light transmittance and decreases the photocatalytic efficiency. Fig. 5(b) presents the relationship between the degradation efficiency of RhB and exposure time within 4.5 h by adding 300 mg of ZnO powder to 20 mL of the RhB solution with different concentrations. By increasing the concentration of RhB, the degradation ratio first increases slightly and then decreases. The degradation efficiency of the RhB solution with a concentration of 15 mg·L^{-1} is remarkable and up to 97.6% with the addition of 300 mg of ZnO to 20 mL of a 15 mg·L^{-1} RhB solution. Under the same conditions, the degradation efficiencies of 10 and 12.5 mg·L^{-1} RhB were nearly the same, reaching 97.2%. An excess of RhB reduces the light transmittance and even covers the active sites on the ZnO particle surface such that the photocatalytic efficiency of RhB is less. When the concentration of RhB is 25 mg·L^{-1}, the degradation efficiency is only 85.4%. Flower-like ZnO demonstrates the available photocatalytic activity in sunshine.

UV–Vis absorption spectra and photoluminescence (PL) spectra of the flower-like ZnO microstructures were recorded at room temperature, as shown in Fig. 6.

As shown in Fig. 6, all of the flower-like ZnO structures show exciton absorption at a wavelength of 288 nm. In Fig. 6(a), a conspicuous mutation in the absorption curve of flower-like ZnO at 382 nm is observed, which may be attributed to the intrinsic band gap absorption because of electron transitions from the valence to conduction band [33–34]. However, it is relatively weak for flower-like ZnO structures growing and destructed structures at 380 and 377 nm, re-

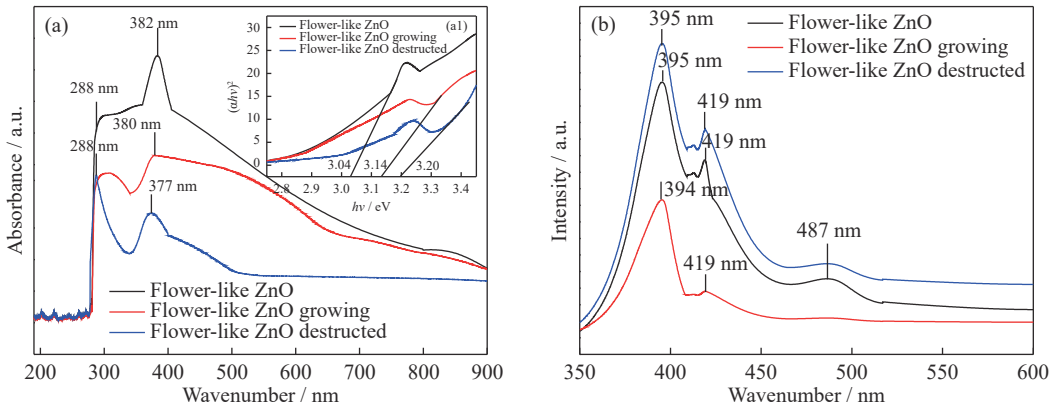

Fig. 6. UV–Vis adsorption spectra (a) and PL spectra (b) of the flower-like ZnO microstructures (a1 in a is the estimated band gap; α is adsorption coefficient, $h\nu$ is photon energy).

spectively. The estimated band gap energies were approximately 3.04, 3.14, and 3.20 eV for the flower-like ZnO structures, flower-like ZnO structures growing and destructed, respectively. All of the calculated band gap energies were less than the theoretical band gap value of 3.37 eV, which may be because of impurity doping from the $ZnSO_4/(NH_4)_2SO_4$ solution used in the synthesis [34]. In the PL spectra obtained with an excitation wavelength of 325 nm, there is a strong UV emission at 395 nm for all of the flower-like ZnO structures because of the near band edge emission [34]. The emission peaks at 419 and 487 nm in the visible region may be assigned to deep level emission because of the oxygen and zinc vacancies [34]. The flower-like ZnO microstructures may serve as UV light-emitting materials; however, the emission peak at 487 nm is not clear for growing flower-like ZnO structures.

The stability of the flower-like ZnO was tested over four cycles and within 60 d of preserved time. As shown in Fig. 7(a), the photocatalytic activity is relatively stable and a slight decrease of 3.5% in the photocatalytic efficiency was observed after four cycles. There was no significant difference in the RhB photocatalytic efficiency of ZnO powder preserved within 30 or 60 d (Fig. 7(b)). However, a decrease of 3.3% was observed with the ZnO powder preserved for 60 d, which may be attributed to the agglomeration caused by absorbing moisture.

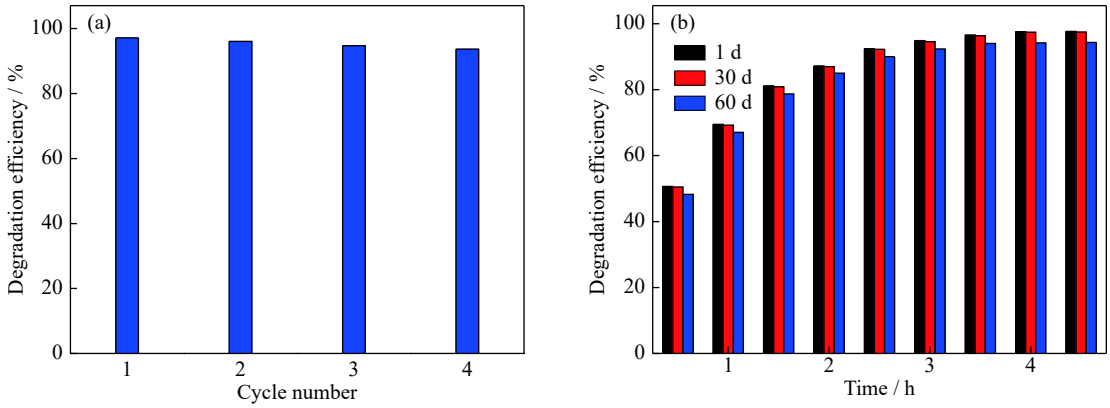

Fig. 7. Relationships between the degradation efficiency of (a) RhB and cycle number and (b) RhB and exposure time by ZnO preserved for up to 60 d.

3.6. Growth mechanism and photocatalytic mechanism

Fig. 8 shows the SEM image and Energy dispersive X-ray spectroscopy (EDS) pattern of the tips of the ZnO rods. The polar growth of the ZnO rods was obvious as observed by the stepped surface. The EDS pattern confirms Zn and O are the main elements. The Au is from the gold coating applied for imaging. No other elements were detected.

Nucleation and crystal growth are the two stages of crystal formation [1,4]. For flower-like ZnO, the formed ZnO nuclei grew to granulum crystals driven by surface energy. Granulum crystals in a supersaturated solution dynamically grow to larger particles. The (001) plane is the close packed plane in the hexagonal system, where growth along the c-axis is energy efficient [4,9]. Furthermore, the positive polar plane of the polar crystal ZnO is Zn^{2+} dominant and the negative plane is O^{2-} dominant [1,4]. The top surfaces were Zn terminated and active, resulting in ZnO rods growing radiatively [1]. Furthermore, the negatively-charged bundles of mi-

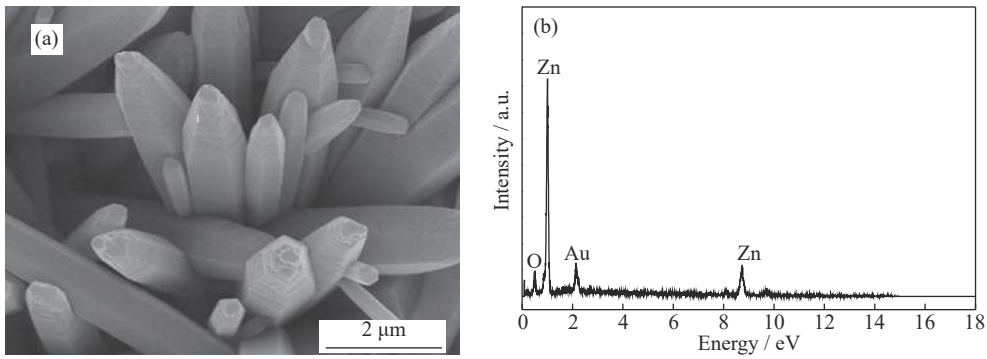

Fig. 8. SEM image (a) and EDS (b) pattern of the ZnO rod.

celles released by SDBS were attracted with the positively-charged Zn^{2+}, affecting the dehydration of $Zn(OH)_4^{2-}$ and promoting ZnO rod growth in bunches to form flower-like ZnO crystals. The growth of ZnO powder can be simply described by Eqs. (1)–(4) [1,4]. The growth process of flower-like ZnO crystals is schematically described in Fig. 9.

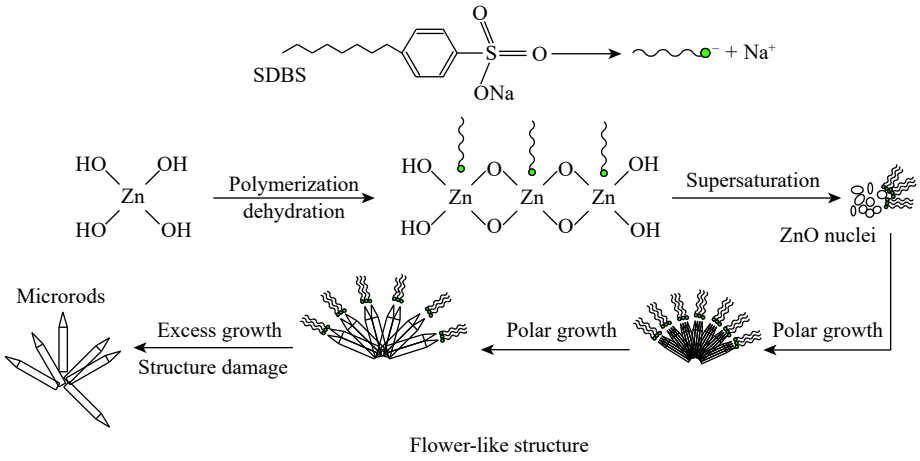

Fig. 9. Schematic of the growth of flower-like ZnO crystals.

$$Zn(CH_3COO)_2 \rightarrow Zn^{2+} + 2CH_3COO^- \quad (1)$$

$$Zn^{2+} + 2OH^- \rightarrow Zn(OH)_2 \quad (2)$$

$$Zn(OH)_2 + 2OH^- \rightarrow Zn(OH)_4^{2-} \quad (3)$$

$$Zn(OH)_4^{2-} \rightarrow ZnO + H_2O + 2OH^- \quad (4)$$

The most energetically active surfaces with terminated Zn^{2+} have many active sites, which are beneficial to photocatalysis. Moreover, the flower-like morphology with a large specific surface area can effectively prevent particle agglomeration, which also contributes to photocatalysis [2]. The major active species of •OH radicals have strong oxidative ability and can oxidize RhB into CO_2 and H_2O [16–17]. Chang *et al.* [35] evidenced the characteristics of •OH radicals by electron paramagnetic resonance (EPR) spectroscopy employing 5,5-dimethylpyrroline-*N*- oxide (DMPO). Moreover, the •OH radicals generated on various photocatalysts were quantitatively investigated by Xiang *et al.* [36]. Under irradiation, excited electrons (e^-) and holes (h^+) in the valence band were obtained by absorbing photons with energy greater than the band gap. The combination of the holes with H_2O and –OH generate •OH radicals, which enhances the photocatalytic reaction, leading to high photocatalytic activity [17,37–38]. The photocatalytic equations are [10,15,37–38]:

$$ZnO + h\nu(UV) \rightarrow ZnO(h^+ + e^-) \quad (5)$$

$$h^+ + H_2O \rightarrow \bullet OH + H^+ \quad (6)$$

$$OH^- + h^+ \rightarrow \bullet OH \quad (7)$$

$$h^+ / \bullet OH + Rhb \rightarrow CO_2 + H_2O \quad (8)$$

4. Conclusions

(1) All of the conditions of hydrothermal temperatures, OH^-/Zn^{2+} molar ratios, time, and amount of dispersant had obvious effects on the micromorphology of the ZnO particles. Flower-like structures were destructed when the hydrothermal temperature, OH^-/Zn^{2+} molar ratio, and hydrothermal time were too high. The parameters for synthesizing flower-like ZnO microstructures were a hydrothermal temperature of 160°C, a OH^-/Zn^{2+} ratio of 5:1, a time of 4 h, and

micelle action with 4 mL of a 5% mass fraction SDBS solution.

(2) The synthesized flower-like ZnO had a hexagon wurtzite structure and showed photolytic activity to degrade RhB with an efficiency of 97.6% under sunshine exposure for 4 h. The formation of flower-like ZnO structures involves the formation and dehydration of $Zn(OH)_4^{2-}$, nucleation, and growth of ZnO crystals. The energetically active surfaces of ZnO rods provide active sites benefiting photocatalysis.

Acknowledgements

This work was financially supported by the Funding of Shenyang Ligong University's Research Support Program for High-level Talents (No. 1010147000802) and the National Natural Science Foundation of China (Nos. 52004165 and 51774070).

References

[1] X.Y. Shen, Y. Liang, Y.C. Zhai, and Z.Q. Ning, Shape-controllable synthesis of ultrafine ZnO powders of different morphologies, *J. Mater. Sci. Technol.*, 29(2013), No. 1, p. 44.

[2] Y.X. Guo, S.W. Lin, X. Li, and Y.P. Liu, Amino acids assisted hydrothermal synthesis of hierarchically structured ZnO with enhanced photocatalytic activities, *Appl. Surf. Sci.*, 384(2016), p. 83.

[3] X.R. Zhang, M. Shakeel, B.S. Li, J.X. Zhang, and L. Wang, Synthesis of foamed zinc oxide–silica spheres coupled with g-C_3N_4 nanosheets for visible light photocatalysis, *J. Mater. Sci.*, 54(2019), No. 20, p. 13118.

[4] M. Gusatti, D.A.R. Souza, N.C. Kuhnen, and H.G. Riella, Growth of variable aspect ratio ZnO nanorods by solochemical processing, *J. Mater. Sci. Technol.*, 31(2015), No. 1, p. 10.

[5] P.V. Adhyapak, S.P. Meshram, D.P. Amalnerkar, and I.S. Mulla, Structurally enhanced photocatalytic activity of flower-like ZnO synthesized by PEG-assited hydrothermal route, *Ceram. Int.*, 40(2014), No. 1, p. 1951.

[6] T.Z. Liu, Y.Y. Li, H. Zhang, M. Wang, X.Y. Fei, S.W. Duo, Y. Chen, J. Pan, and W. Wang, Tartaric acid assisted hydrothermal synthesis of different flower-like ZnO hierarchical architectures with tunable optical and oxygen vacancy-induced photocatalytic properties, *Appl. Surf. Sci.*, 357(2015), p. 516.

[7] M. Sheikh, M. Pazirofteh, M. Dehghani, M. Asghari, M. Rezakazemi, C. Valderrama, and J.L. Cortina, Application of ZnO nanostructures in ceramic and polymeric membranes for water and wastewater technologies: A review, *Chem. Eng. J.*, 391(2020), art. No. 123475.

[8] M. Laurenti, S. Stassi, G. Canavese, and V. Cauda, Surface engineering of nanostructured ZnO surfaces, *Adv. Mater. Interfaces*, 4(2017), No. 2, art. No. 1600758.

[9] S.W. Duo, Y.Y. Li, H. Zhang, T.Z. Liu, K. Wu, and Z.Q. Li, A facile salicylic acid assisted hydrothermal synthesis of different flower-like ZnO hierarchical architectures with optical and concentration-dependent photocatalytic properties, *Mater. Charact.*, 114(2016), p. 185.

[10] M.J. Cao, F. Wang, J.F. Zhu, X. Zhang, Y. Qin, and L. Wang, Shape-controlled synthesis of flower-like ZnO microstructures and their enhanced photocatalytic properties, *Mater. Lett.*, 192(2017), p. 1.

[11] T.T. Jiang, Y.Q. Wang, D.W. Meng, X.L. Wu, J.X. Wang, and J.Y. Chen, Controllable fabrication of CuO nanostructure by hydrothermal method and its properties, *Appl. Surf. Sci.*, 311(2014), p. 602.

[12] M. Dhiman, R. Sharma, V. Kumar, and S. Singhal, Morphology controlled hydrothermal synthesis and photocatalytic properties of $ZnFe_2O_4$ nanostructures, *Ceram. Int.*, 42(2016), No. 11, p. 12594.

[13] A. Ulyankina, I. Leontyev, M. Avramenko, D. Zhigunov, and N. Smirnova, Large-scale synthesis of ZnO nanostructures by pulse electrochemical method and their photocatalytic properties, *Mater. Sci. Semicond. Process.*, 76(2018), p. 7.

[14] X.Y. Shen, Y.J. Shi, H.M. Shao, Y. Liu, and Y.C. Zhai, Synthesis and photocatalytic degradation ability evaluation for rhodamine B of ZnO@SiO_2 composite with flower-like structure, *Water Sci. Technol.*, 80(2019), No. 10, p. 1986.

[15] X.Y. Shen, H.M. Shao, Y. Liu, and Y.C. Zhai, Synthesis and photocatalytic performance of ZnO with flower-like structure from zinc oxide ore, *J. Mater. Sci. Technol.*, 51(2020), p. 1.

[16] S.M. Lam, M.W. Kee, and J.C. Sin, Influence of PVP surfactant on the morphology and properties of ZnO micro/nanoflowers for dye mixtures and textile wastewater degradation, *Mater. Chem. Phys.*, 212(2018), p. 35.

[17] H.S. Zhou, H.J. Zhang, Y. Wang, Y. Miao, L.B. Gu, and Z. Jiao, Self-assembly and template-free synthesis of ZnO hierarchical nanostructures and their photocatalytic properties, *J. Colloid Interface Sci.*, 448(2015), p. 367.

[18] C.S. Lei, M. Pi, W. Zhou, Y.Q. Guo, F.G. Zhang, and J.Q. Qin, Synthesis of hierarchical porous flower-like ZnO–AlOOH structures and their applications in adsorption of congo red, *Chem. Phys. Lett.*, 687(2017), p. 143.

[19] P. Dhatshanamurthi and M. Shanthi, Enhanced photocatalytic degradation of azo dye in aqueous solutions using Ba@Ag@ZnO nanocomposite for self-sensitized under sunshine irradiation, *Int. J. Hydrogen Energy*, 42(2017), No. 8, p. 5523.

[20] P.Y. Gong, B.S. Li, X.L. Kong, M. Shakeel, J.J. Liu, and S.L. Zuo, Hybriding hierarchical zeolite with Pt nanoparticles and graphene: Ternary nanocomposites for efficient visible-light photocatalytic degradation of methylene blue, *Microporous Mesoporous Mater.*, 260(2018), p. 180.

[21] A. Raza, H.L. Shen, A.A. Haidry, and S.S. Cui, Hydrothermal synthesis of Fe_3O_4/TiO_2/g-C_3N_4: Advanced photocatalytic application, *Appl. Surf. Sci.*, 488(2019), p. 887.

[22] J. Liu, P.L. Wang, W.Q. Qu, H.R. Li, L.Y. Shi, and D.S. Zhang, Nanodiamond-decorated ZnO catalysts with enhanced photocorrosion-resistance for photocatalytic degradation of gaseous toluene, *Appl. Catal. B*, 257(2019), art. No. 117880.

[23] Y.Q. Wang, T.T. Jiang, D.W. Meng, J. Yang, Y.C. Li, Q. Ma, and J. Han, Fabrication of nanostructured CuO films by electrodeposition and their photocatalytic properties, *Appl. Surf. Sci.*, 317(2014), p. 414.

[24] Q. Chen, Y.Q. Wang, M.Y. Zheng, H. Fang, and X. Meng, Nanostructures confined self-assembled in biomimetic nanochannels for enhancing the sensitivity of biological molecules response, *J. Mater. Sci. Mater. Electron.*, 29(2018), No. 23, p. 19757.

[25] A. Kar, J. Olszówka, S. Sain, S.R.I. Sloman, O. Montes, A. Fernández, S.K. Pradhan, and A.E.H. Wheatley, Morphological effects on the photocatalytic properties of SnO_2 nanostructures, *J. Alloys Compd.*, 810(2019), art. No. 151718.

[26] L.P. Wang, F. Zhang, S. Chen, and Z.H. Bai, One-pot synthesis

and optical properties of In- and Sn-doped ZnO nanoparticles, *Int. J. Miner. Metall. Mater.*, 24(2017), No. 4, p. 455.

[27] J.C. Yao, M. Zhang, H.F. Yin, Y.T. Luo, and X.H. Liu, Improved photocatalytic activity of WO_3/C_3N_4: By constructing an anchoring morphology with a Z-scheme band structure, *Solid State Sci.*, 95(2019), art. No. 105926.

[28] Y. Bao, C. Wang, and J.Z. Ma, Morphology control of ZnO microstructures by varying hexamethylenetetramine and trisodium citrate concentration and their photocatalytic activity, *Mater. Des.*, 101(2016), p. 7.

[29] S.M. Mousavi, A.R. Mahjoub, and R. Abazari, Facile green fabrication of nanostructural Ni-doped ZnO hollow sphere as an advanced photocatalytic material for dye degradation, *J. Mol. Liq.*, 242(2017), p. 512.

[30] T.V.A. Kusumam, T. Panakkal, T. Divya, M.P. Nikhila, M. Anju, K. Anas, and N.K. Renuka, Morphology controlled synthesis and photocatalytic activity of zinc oxide nanostructures, *Ceram. Int.*, 42(2016), No. 3, p. 3769.

[31] J.X. Zhan, H.X. Dong, Y. Liu, Y.L. Wang, Z.H. Chen, and L. Zhang, A novel synthesis and excellent photodegradation of flower-like ZnO hierarchical microspheres, *CrystEngComm*, 15(2013), No. 47, p. 10272.

[32] N. Rana, S. Chand, and A.K. Gathania, Synthesis and characterization of flower-like ZnO structures and their applications in photocatalytic degradation of rhodamine B dye, *J. Mater. Sci. Mater. Electron.*, 27(2016), No. 3, p. 2504.

[33] Y.Q. Wang, Q. Ma, H.X. Jia, and Z.S. Wang, One-step solution synthesis and formation mechanism of flower-like ZnO and its structural and optical characterization, *Ceram. Int.*, 42(2016), No. 9, p. 10751.

[34] X.Z. Lv, X.C. Liu, Q.M. Sun, Y.Q. Wang, and B. Yan, Growth and optical properties of hierarchical flower-like ZnO nanostructures, *Ceram. Int.*, 43(2017), No. 3, p. 3306.

[35] S.M. Chang, P.H. Lo, and C.T. Chang, Photocatalytic behavior of TOPO-capped TiO_2 nanocrystals for degradation of endocrine disrupting chemicals, *Appl. Catal. B*, 91(2009), No. 3-4, p. 619.

[36] Q.J. Xiang, J.G. Yu, and P.K. Wong, Quantitative characterization of hydroxyl radicals produced by various photocatalysts, *J. Colloid Interface Sci.*, 357(2011), No. 1, p. 163.

[37] Y. Zhang, J.B. Zhou, Z. Li, and Q.Q. Feng, Photodegradation pathway of rhodamine B with novel Au nanorods@ZnO microspheres driven by visible light irradiation, *J. Mater. Sci.*, 53(2018), No. 5, p. 3149.

[38] X.Y. Zhang, J.Q. Qin, R.R. Hao, L.M. Wang, X. Shen, R.C. Yu, S. Limpanart, M.Z. Ma, and R.P. Liu, Carbon-doped ZnO nanostructures facile synthesis and visible light photocatalytic applications, *J. Phys. Chem. C*, 119(2015), No. 35, p. 20544.